Macromolecules

pubs.acs.org/Macromolecules Article

Structure of Polymer Rings in Linear Matrices: SANS Investigation

Margarita Kruteva,* Michael Monkenbusch, Jürgen Allgaier, Wim Pyckhout-Hintzen, Lionel Porcar, and Dieter Richter

Cite This: *Macromolecules* 2023, 56, 4835−4844 Read Online

ACCESS | Metrics & More | Article Recommendations

ABSTRACT: We have presented a systematic small angle neutron scattering investigation of ring−linear blends, where we vary either the ring volume fraction for a given ring in a long linear matrix or the matrix length at a low ring fraction. We found that the ring radius of gyration (R_g) shrinks with increasing ring fraction and nearly reaches the R_g of the ring melt at a volume fraction of $\phi_R = 0.5$. At the same time, the fractal dimension, which is close to a Gaussian conformation at low ϕ_R, decreases to the value of the ring melt. Aside from very short matrices, the ring size is independent of the host length. Following a random phase approximation treatment, the effective Flory−Huggins parameter ($\chi_{F,RL}$) is negative and independent of ϕ_R, signifying ring−linear attraction that leads to ring−ring repulsion. $\chi_{F,RL}$ decreases with decreasing ring size, which might be related to the decreasing possibility of threading events, when the ring size becomes smaller. The ϕ_R-dependent data in the cross-over regime between low Q Porod scattering $\sim Q^{-4}$ and polymer RPA contribution displays an intermediate Q^{-2} regime, the intensity of which increases proportional to ϕ_R. The origin of this Q^{-2} contribution is not clear but may be related to critical fluctuations or microphase separation induced by a nonlocal positive contribution to $\chi_{F,RL}$. The experimental results fit well into the general picture that is mainly based on simulations, even though in detail, quantitative differences are obvious. Finally, our results are in qualitative agreement with earlier studies on polystyrene ring−linear blends.

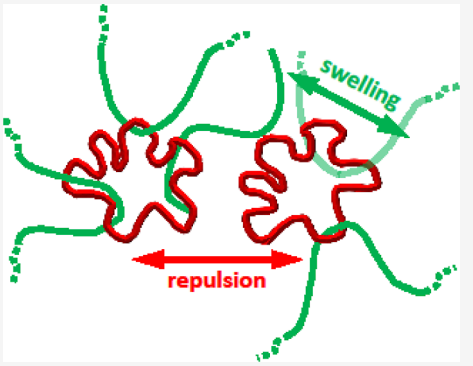

INTRODUCTION

Among all polymer architectures, the topology of polymer rings is unique as they are the simplest closed structures without ends. For instance, while in the melt, linear chains interpenetrate easily, for ring polymers, interpenetration is entropically costly and compact structures that evolve for high molecular weight become mass fractals confining rings into territories.[1,2] On the local scale, the formation of loops was predicted. Size and conformation of loops, as well as their dependence on the molecular weight of the ring, have been a focus of the theoretical discussions since a few decades.[3−6] Recently, a clear signature of the predicted elementary loops that build the ring conformation has been shown experimentally.[7]

Blending rings with linear chains strongly affects both the ring structure and dynamics. As a consequence of threading by linear chains, the ring structure changes, and its diffusivity is strongly reduced. In the molecular dynamics (MD) simulation work of Tsalikis and Mavrantzas, a detailed analysis of threading events was performed.[8] They found that in the dilute limit ($\phi_R = 0.1$), all rings are threaded by linear chains at least once and no ring−ring threading is observed. On average, the number of threadings is nearly independent of the matrix chain length. The ring conformation was found to be swollen in the linear matrix and the degree of swelling is larger for shorter linear matrix chains; thereby, the size of the linear host is not affected. The simulations indicated that the ring swelling appears to be more pronounced for shorter hosts. Ring−linear threadings were identified as the key mechanism that governs the size, the conformation, and the dynamics of ring−linear blends.[8,9] In terms of coarse-grained bead-spring simulations investigating ring and linear chains of 400 beads, Grest et al. studied the ring conformation and dynamics of ring−linear blends from the neat ring to the neat linear polymer melt.[10] They found that ring−linear threadings enable ring polymers to topologically entangle with other rings and with the entanglement network of the linear chains, inducing large changes in the equilibrium conformation and dynamics of the rings. While both the Mavrantzas group and Grest counted a large number of ring−linear threadings, Hagita and Murashima in their bead-spring simulation found much smaller average threading events.[11] The ring swelling was found to be a nonlinear function of the number of penetrations with no

Received: December 2, 2022
Revised: April 24, 2023
Published: June 28, 2023

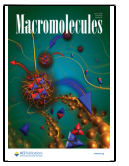

https://doi.org/10.1021/acs.macromol.2c02444
Macromolecules 2023, 56, 4835−4844

influence from the linear host size. Furthermore, they present a power−law relationship between ring swelling and ring volume fraction $R_{g,R}^2 \sim \phi_R$ with $0.06 \leq \alpha \leq 0.09$, where the higher exponent is related to the larger ring.

Aside from the MD simulations, Monte-Carlo simulations are also reported.[12] They also found large numbers of threadings, agreeing with Mavrantzas' atomistic MD simulations. Again, except for very short hosts, the number of threadings is rather independent of the linear host size. Iyer et al. presented a scaling model to capture the ring swelling, describing the linear host as a theta-solvent for a semidilute ring fraction.[13] According to this approach, rings swell most as long as they do not overlap; above the overlap concentration, deswelling occurs following a power law $R_{g,R} \sim \phi_R^{\beta}$; $\beta = 2\nu - 1$, where ν is the fractal exponent describing the ring conformation. Finally, based on atomistic MD simulations of ring−linear polyethylene blends, Jeong and Douglas question the threading effect and ascribe ring swelling to a topology-induced excluded volume interaction predicting a scaling relation $\langle R_{g,R}^2 \rangle = \langle R_{g,R}^2 \rangle_0 (1 + \alpha \phi_R/\phi_R^*)^{\beta}$ and $\beta = 2(1 - 3\nu_0)/(\nu_0 - \nu_{melt})$, with ϕ_R^* being the overlap concentration; ν_0 the fractal ring exponent for $\phi_R \ll \phi_R^*$; α the prefactor; and ν_{melt} the fractal exponent in the ring melt.[14]

The most detailed experimental study on the conformation of sizable rings blended in a linear matrix was presented by Iwamoto et al.[15] They investigated polystyrene ring−linear blends by varying the molecular weight of the host from 22.4 kDa to 270 kDa, while the ring size was kept constant at 70 kDa. They observed a gradual swelling of rings with an increasing amount of linear polymer. The molecular weight of the host had, if at all, little influence on the degree of swelling. Ring swelling was described by a power−law relationship as $R_{g,R}^2 \sim \phi_R^{-0.1 \pm 0.03}$; even at $\phi_R = 0.2$, $R_{g,R}$ was found to be still smaller than that of a Gaussian ring. There are also a few studies on ring−linear systems of unlike polymers,[16,17] which, however, are beside the focus of this research.

Many questions are still open: (i) experimental and simulation studies of ring−linear blends have just touched the details of ring threading. The conformation and dynamics of rings in a blend as a function of ring size and linear matrix length are not fully explored yet. (ii) It is unknown how the structure, dynamics, and rheology of ring−linear blends change as a function of ring concentration. (iii) There are some indications for a ring−linear phase separation that, however, are not covered by theoretical prediction; the physics of such a topological phase separation driven by a strongly nonlocal interaction parameter would be highly exciting and needs to be explored.

In this work, we focus on the conformation and interaction of polymer rings in ring−linear blends measured by small angle neutron scattering (SANS). Using isotope labeling, we have highlighted the rings vs the linear host. The investigations went in two directions: (i) the concentration dependence of the ring conformation in a long linear matrix and (ii) the dependence of the ring conformation on the host matrix length at low ring volume fraction. The following results stand out: (1) ring−linear blends display a strong negative chi-parameter indicating attraction between ring and linear chains; (2) the ring radius of gyration follows a power law in the ring volume fraction $R_{g,R}^2 \sim \phi_R^{-0.2}$; and (3) $R_{g,R}$ is independent of the host matrix length.

Theoretical Considerations. In our previous work, we studied the conformation of large molecular weight rings in the melt. The SANS data were interpreted in terms of a self-similar form factor of a ring that is built from elementary loops. The size of these loops came out as being close to that of an entanglement strand in the corresponding linear melt. The SANS data displayed a clear cross-over from the larger-scale fractal structure to Gaussian loops at shorter distances. The size of these elementary loops was found to be independent of the ring molecular weight. We modeled the ring form factor in terms of an expression by Bensafi et al.[18] Additionally, we included the cross-over from the fractal structure at larger scales to a Gaussian loop structure at shorter distances. At larger distances along the ring contour length, *i.e.*, small values of wave vector Q, we expect compressed fractal conformations. There, the real space distances r_{ij} between monomers i and j relate to a random walk more compact than Gaussian with a fractal dimension $d_f = \frac{1}{\nu}$, where ν is the expansion exponent

$$\langle r_{ij}^2 \rangle \sim \left((|i - j|) \left(1 - \frac{|i - j|}{N_R} \right) \right)^{2\nu} \tag{1}$$

The form factor is calculated by direct summation over all N_R segments of the ring with a change of statistics as a function of distance along the chain. The second term in eq 1 represents the ring closure condition. For $|i-j| \leq N_{e,0}$, where $N_{e,0}$ is the loop size, the loop statistics is expressed by $\nu = \frac{1}{2}$ and is Gaussian. For the larger-scale $|i-j| > N_{e,0}$, the fractal exponent ν becomes smaller than 1/2 and eventually for large N_R, we should assume the mass fractal exponent $\nu = \frac{1}{3}$. The shape of the cross-over between both regimes was described by a Fermi function of width ν_{width} centered at $N_{e,0}$. Then, the ring form factor becomes

$$P_R(Q) = \frac{1}{N_R} \sum_{i,j}^{N_R} \exp\left[-\frac{Q^2 l^2}{6} |i - j|^{2\nu_{eff}} \left(1 - \frac{|i - j|}{N} \right)^{2\nu_{eff}} \right] \tag{2}$$

with

$$\nu_{eff} = \nu_1 + \left(\frac{\nu - \nu_1}{1 + \exp\left(\frac{N_{e,0} - |i - j|}{\nu_{width}} \right)} \right) \tag{3}$$

where $\nu_1 = \frac{1}{2}$ is the local chain expansion exponent, $\nu = 1/d_f$ is the large-scale (fractal) exponent, and l is a monomer length.

In order to describe the two components in the melt of rings and linear chains, we used the random phase approximation (RPA) approach. The ring structure factor for a binary melt of rings and linear polymers in the RPA model is given by[19]

$$S_{RPA}(Q) = \frac{S_{RR}^0(Q)}{1 + \nu_{RR}(Q) S_{RR}^0(Q)} \tag{4}$$

where $S_{RR}^0(Q) = {}_R\phi N_R P_R(Q)$ determines the form factor of the ring and $\nu_{RR}(Q)$ is the interaction term

$$\nu_{RR}(Q) = \frac{1}{S_{LL}^0(Q)} - 2\chi_{F,RL} \tag{5}$$

with $S_{LL}^0(Q) = (1 - \phi_R) N_L P_L(Q)$ being the form factor of the linear chain taken as the Debye function. The conventional Flory−Huggins parameter describes the interaction between two linear polymers without taking into account topological

https://doi.org/10.1021/acs.macromol.2c02444
Macromolecules 2023, 56, 4835−4844

interactions. To distinguish, we use an effective Flory–Huggins parameter $\chi_{F,RL}$ describing the interaction between the ring and linear polymer including topological effects. Finally, the macroscopic neutron cross-section in (cm^{-1}) observed in a small angle scattering experiment becomes

$$I(Q) \equiv \frac{d\Sigma}{d\Omega} = V_W \Delta\rho^2 S_{RPA}(Q) \quad (6)$$

with V_W being the polymer volume (cm^3 mol^{-1}); $\Delta\rho = [N_A n(b_D - b_H)]/\Omega_0$; N_A the Avogadro number; n the number of hydrogens/deuterons contained in the monomer; b_D and b_H the neutron scattering lengths for deuteron and hydrogen; and Ω_0 the monomer volume (cm^3 mol^{-1}).

Synthesis and Characterization. The synthesis of the polyethylene-oxide (PEO) ring and linear polymers is described in detail elsewhere.[7,20,21] The molecular weights and their distribution in terms of M_w/M_n of the investigated polymers are given in Tables 1 and 2. The samples were blended in toluene solution and freeze-dried afterward; finally, the materials were hot pressed to obtain 1 mm sample foils, which were then filled into the flat Hellma cuvettes of 10 mm width and 1 mm thickness in an inert atmosphere. The compositions of the blends are presented in Table 3. In the case of the 40 K ring, the rings were deuterated, while the linear chains were hydrogenated. In all the other cases, hydrogenated rings were blended with a deuterated linear matrix.

Table 1. Molecular Weights of the Rings $M_{n,R}$, the Degree of Polymerization or the Respective Numbers of Monomers N_R, the Ratio of N_R and Entanglement Length $N_{e,0} = 45$, and the Corresponding Polydispersities $(M_w/M_n)_R$[a]

	h-10K [g/mol]	h-20K [g/mol]	d-40K [g/mol]
$M_{n,R}$	10,100	20,100	38,600
monomer number N_R	230	456	804
N_R/N_e	5	10	18
$(M_w/M_n)_R$	1.03	1.03	1.01

[a]"h" denotes hydrogenated and "d" deuterated polymers, respectively.

METHODS

SANS experiments on the concentration series R40L100 at different volume fractions were carried out on the SANS instrument D22[24] at the Institute Laue Langevin (ILL) in Grenoble, France, at a temperature of 413K, neutron wavelengths of 0.6 and 1.2 nm, and sample-to-detector lengths of 2, 11.2, and 17.6 m.[25] R10/L80, R20/L20, R20/L80, and R20/L2 were measured on the instrument SANS-II at the Paul Scherrer Institut (PSI) in Villigen, Switzerland, at a temperature of 413 K, a neutron wavelength of 0.47 nm, and sample-to-detector lengths of 6.3 and 1.05 m.[26] The sample R20/L200 was measured on a KWS-1 instrument at the Heinz Maier-Leibnitz Zentrum (MLZ) in Munich, Germany, at a temperature of 413K, a neutron wavelength of 0.45 nm, and sample-to-detector lengths of 1.3, 7.8, and 19.8 m.[27] The two-dimensional SANS data were orientationally averaged, background subtracted, and normalized to absolute scale using direct beam measurements. Data from adjacent Q-values were merged according to their statistical errors. The amount of incoherent scattering was fitted as a constant additional background and then subtracted from the data.

Table 3. Composition of the Investigated Blends (Weight % of Rings)

R/L	L2	L20	L80	L100	L200
R10	16		15		
R20	10	10	10		10
R40				10, 20, 35, 50	

RESULTS

We have investigated the conformation of ring–linear polymer blends focusing on the following:

(i) the conformational changes of a large 40 K ring in a blend with a 100 K linear polymer as a function of ring concentration.
(ii) the conformation of a 20 K ring at a volume fraction of 10 ww % as a function of the molecular weight of the host linear matrix.

In all cases, by choosing a proper h/d contrast, the rings were highlighted and the SANS data reflect the ring conformation, however, modified by RPA contributions.

We start with the concentration-dependent conformation: Figure 1 displays the results. The SANS data show a typical polymer form factor with a Q^{-2} decay at high Q and a near Guinier plateau at intermediate Q. Toward low Q, we observe a strong increase in the forward scattering following a Porod Q^{-4} behavior. As we shall discuss later, in the regime between the form factor and the Porod scattering, a second Q^{-2} regime emerges.

Involving the ring form factor of Eqs 1 and 2 and employing the RPA approach described by eqs 4 and 5, the data were fitted. The low Q behavior was described by a combination of a Q^{-2} and a Q^{-4} term. Following earlier studies, many parameters are known. Therefore, in the fits, only the intensity parameter, the fractal exponent ν, and the effective Flory–Huggins parameter $\chi_{F,RL}$ were varied. In addition, the amplitudes of the Q^{-2} and Q^{-4} contributions were fitted. In general, the fits are excellent and describe the data over the full Q-range very well. We note that a Porod contribution alone does not describe the low Q spectral part. We discuss this phenomenon later in detail. Table 4 presents the thus obtained parameters. The ring radius of gyration $R_{g,R}$ was calculated based on the form factor of eq 2. Finally, the errors given are

Table 2. Molecular Weights of the Linear Chains $M_{n,L}$, the Degree of Polymerization or the Respective Numbers of Monomers N_L, the Ratio of the Chain Length and Entanglement Length $N_{e,0} = 45$, and the Corresponding Polydispersities $(M_w/M_n)_L$[a]

	d-2K [g/mol]	d-20K[22] [g/mol]	d-80K [g/mol]	h-100K [g/mol]	d-200K[23] [g/mol]
$M_{n,L}$	1941	22,236	90,000	100,500	207,300
monomer number N_L	41	484	1875	2284	4320
N_L/N_e	<1	11	42	51	96
$(M_w/M_n)_L$	1.05	1.05	1.05	1.01	1.04

[a]"h" denotes hydrogenated and "d" deuterated polymers, respectively.

https://doi.org/10.1021/acs.macromol.2c02444
Macromolecules 2023, 56, 4835−4844

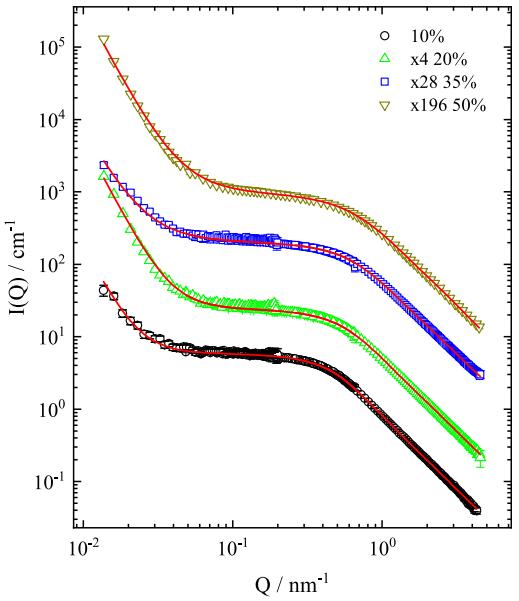

Figure 1. SANS results from the blends of a 40 K PEO ring in a 100 K linear PEO matrix at various ring volume fractions ϕ_R: 10, 20, 35, and 50 ww %. The data for 20, 35, and 50 ww % are shifted by a factor of 4, 28, and 196, respectively. The lines display the fitting results (see text). Note: the scattering profiles contain via RPA contributions of the linear host.

the statistical errors; any possible systematic errors are not included.

We observe that (i) the fractal exponent ν decreases with an increasing ring volume fraction, reaching the value of the pure ring melt at ϕ_R = 50 ww %; (ii) the effective Flory–Huggins parameter $\chi_{F,RL}$ is always negative and, within the errors, independent of the ring fraction ϕ_R; (iii) the coefficient of the Porod term a4 varies unsystematically with ϕ_R, (iv) while the Q^{-2} contribution grows in proportion to the ring fraction; and (v) finally, the ring radius of gyration decreases significantly with increasing ϕ_R and, at ϕ_R = 50 ww %, nearly assumes the value of the ring melt. Figure 2 presents the dependence of the parameters a2, a4, ν and the ring radius of gyration $R^2_{g,R}(\phi_R)$ on the ring volume fraction.

We have also explored different ring sizes in similar linear matrices (R10/L80, R20/L80, and R40/L100) (Figure 3a) and the R20 ring in linear matrices of different lengths (L2, L20, L40, L80, and L200) (Figure 3b) (see Tables 4 and 5). The ring volume fractions ϕ_R in the different linear hosts determining the composition of the blend are presented in Table 3. With an exception for R10 and R40, the ring concentration was 10 ww %. Some of the data were taken from earlier measurements and were partially published in a different context.[22] Again, the data were fitted with the RPA model, and the resulting parameters are displayed in Table 5. Figure 3a compares the SANS data from rings of different sizes in the L80 or L100 matrices, respectively. Figure 3b displays the SANS results for the R20 ring in linear matrices of different sizes.

We remark that some of the older data for R10 and R20 were of lower quality, and the Q-ranges studied varied importantly. Therefore, the Q^{-4} contribution which can be related to the inhomogeneities in the sample volume, *e.g.*, due to the air bubbles, is not present for all samples.

The radii of gyration appear not to depend on the host size. However, for the smallest host (L2), $\chi_{F,RL}$ is significantly smaller than for the longer linear chains. The fractal exponents ν are always close to 0.5—the rings exhibit Gaussian statistics. As it is well known from linear chains, for very short matrices in the oligomer range, the hosts behave as solvent molecules, and swelling of the probe chain is expected.[15,28−34] This situation appears not to occur for our blends—even for the L2 host, the fractal exponent stays at ν = 0.5. The remaining fluctuations of the parameter values are most likely due to the limited quality of the data. The solid lines in Figure 3 present the fitting results. Finally, we note that at an even lower volume fraction (ϕ_R = 1 ww %), the R20 ring in the L20 host leads to more pronounced swelling of the ring molecule of $\frac{R^2_{g,R}}{R^2_{g,R,melt}} = 1.72$ (ϕ_R = 1 ww %)[22] compared to $\frac{R^2_{g,R}}{R^2_{g,R,melt}} = 1.54$ (ϕ_R = 10 ww %) otherwise.

DISCUSSION

Ring Conformation. The scattering function obtained from the RPA does not directly reflect the underlying features of the ring form factor. To clarify how the genuine ring conformation is changing with the ring volume fraction, from the fit parameters displayed in Table 2, we calculated the true ring form factors for the series of ring–linear blends at different ring volume fractions. Figure 4 displays the results in a Kratky representation. From Figure 4, we clearly see that the intermediate peak structure, characterizing the compact ring conformation, develops with increasing ring volume fraction, indicating the fractal-like conformation for the largest ring R40. At ϕ_R = 50 ww %, the ring conformation is already close to that of the ring in its own melt.

Ring Swelling. To characterize the degree of ring swelling in the linear polymer matrix, Figure 2c displays the ϕ_R dependence of the ring size $R^2_{g,R}(\phi_R)$ for the largest ring R40 in the L100 linear matrix in a double-logarithmic plot, resulting in $R^2_{g,R}(\phi_R) \sim \phi_R^{-0.20}$. We note that for a given ring size, the

Table 4. Parameters Obtained by Fitting the Concentration-Dependent Ring–Linear R40/L100 Blend Data: ν: Fractal Ring Exponent (eq 3); $\chi_{F,RL}$: Effective Flory–Huggins Parameter; a4 and a2: Amplitudes Describing the Q^{-4} and Q^{-2} Contributions to the Forward Scattering; $R_{g,R}$: Ring Radius of Gyration; and χ^2: Goodness of the Fit

ϕ_R ww %	ν	$-\chi_{F,RL}$	a4(Q^{-4})/nm^4 cm^{-1}	a2(Q^{-2})/nm^2 cm^{-1}	$R_{g,R}$[a]/nm	χ^2
10	0.484 ± 2.7 × 10^{-4}	0.0142 ± 4.9 × 10^{-5}	1.8 × 10^{-6}± 1.5 × 10^{-7}	0.33 × 10^{-3}± 1.5 × 10^{-4}	4.30 ± 0.01	1.07
20	0.473 ± 2.7 × 10^{-4}	0.0150 ± 3.3 × 10^{-5}	1.3 × 10^{-5}± 1.7 × 10^{-7}	2.57 × 10^{-3}± 1.2 × 10^{-4}	4.07 ± 0.01	1.85
35	0.460 ± 2.9 × 10^{-4}	0.0160 ± 2.7 × 10^{-5}	2.3 × 10^{-6}± 1.4 × 10^{-7}	4.42 × 10^{-3}± 1.2 × 10^{-4}	3.82 ± 0.01	2.14
50	0.451 ± 5.0 × 10^{-4}	0.0156 ± 3.7 × 10^{-5}	1.78 × 10^{-5}± 1.7 × 10^{-7}	8.49 × 10^{-3}± 1.1 × 10^{-4}	3.66 ± 0.01	9.25
100	0.448 ± 3.0 × 10^{-4}				3.54 ± 0.07	

[a]The errors were calculated using eq 4 and evaluating $R_{g,R}$ at the limits for the different model parameters that are defined by the statistical errors. Note that the small errors for $R_{g,R}$ result from the fact that all data points are used in the evaluation of the errors.

https://doi.org/10.1021/acs.macromol.2c02444
Macromolecules 2023, 56, 4835−4844

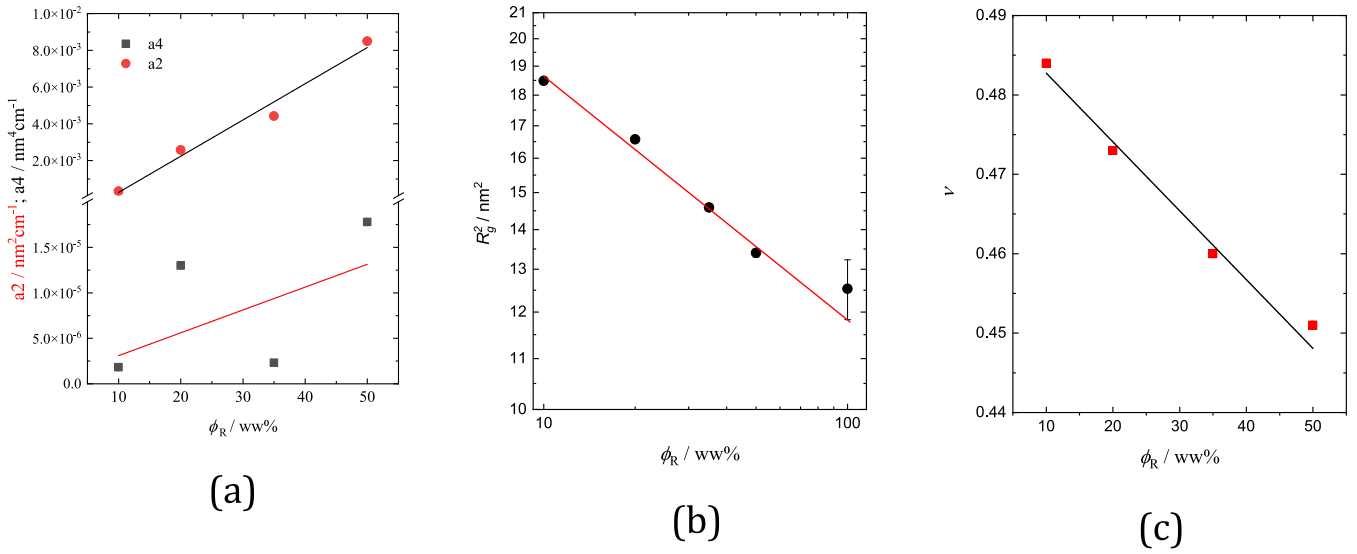

Figure 2. (a) Q^{-4} (a4) and Q^{-2} (a2) contributions to the SANS forward scattering as a function of the R40 ring volume fraction. (b) $R^2_{g,R}(\phi_R)$ *vs* the ring volume fraction ϕ_R in double-logarithmic presentation. The solid line represents a slope −0.20. (c) Fractal exponent ν as a function of the ring volume fraction. In each case, the error bars are smaller than the symbol sizes.

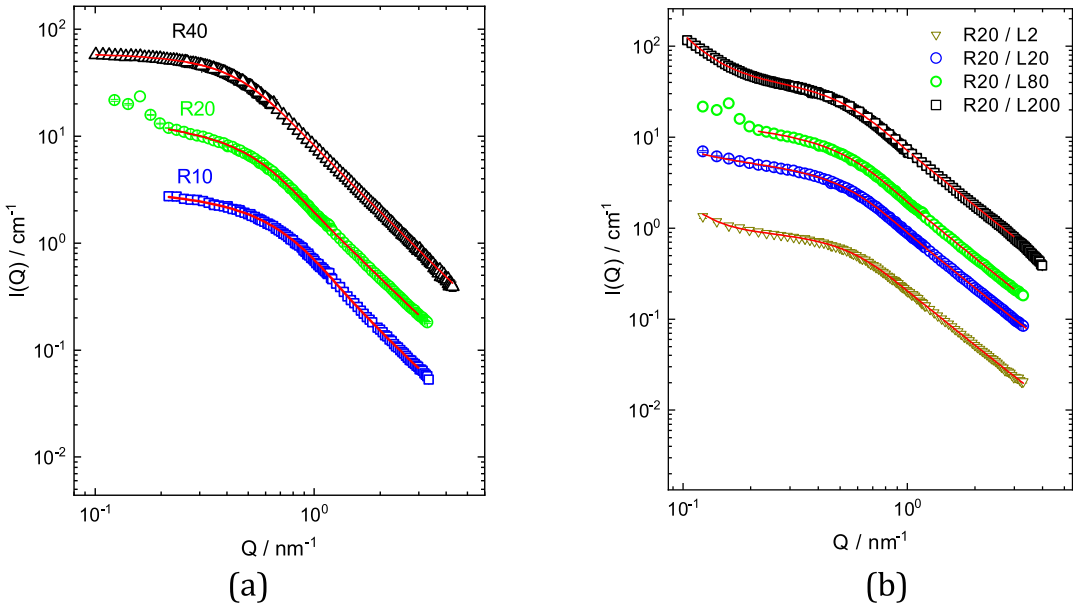

Figure 3. SANS results (a) for rings of different sizes in a long chain linear matrix: R10 in L80, R20 in L80, and R40 in L100. The data for R20 and R40 were shifted by a factor of 2 and 10, respectively; R40 in L100 data was taken at ϕ_R = 10 ww %. (b) R20 ring in matrices of different sizes. From above: L200 (shifted by a factor of 10), L80 (shifted by a factor of 2), L20, and L2. For lines, see text.

degree of swelling was not found to depend on the host (see Table 3 for R20 in different matrices). However, for R20 at a low volume fraction (ϕ_R = 1 ww %), Gooßen et al. observed a larger swelling by about 72% compared to the ring melt. The swelling of the differently sized rings at volume fractions of 10 ww % or 15−16 ww % for the equivalent host matrix amounts to 1.26 for R10; 1.53 for R20; and 1.43 for R40. Apparently, two effects influence the ring swelling behavior in a blend at low ring volume fraction. First, threading of the smallest rings is limited by their size. Therefore, the smallest rings are more compact. Second, the attraction between rings and linear chains slightly increases with ring size ($R10{:}\chi_F \cong -0.013; R20{:}\chi_F \cong -0.013; R40{:}\chi_F \cong -0.016$). The larger ring cross-section with increasing ring size allows for a higher amount of threadings and thus increases the ring-linear attraction by topological means. On the other side, the degree of swelling is rather independent of the linear matrix length.

While for R20/L20, we find a significant swelling of $\frac{R^2_{g,R}}{R^2_{g,R,melt}} = 1.54$ (Table 3), Mavrantzas' atomistic simulations on the PEO system predict that under these conditions, the ring size is equal to that of the melt. Concerning the absolute value of $R_{g,R}$ for the ring melt, the simulations are very close to the experiment: we find $R_{g,R,melt}$ = 2.78 nm compared to 2.87 nm in the simulation. However, the results in the blend are very different (experiment: 3.46 nm and simulation: 2.85 nm). For shorter hosts (R10/L10), the simulations indicate some swelling (R10/L10: 1.07).[8,9] Within statistics, the persistence length between ring and linear are the same (about 0.64 nm), not far from the segment length of 0.568 nm that we found.

https://doi.org/10.1021/acs.macromol.2c02444
Macromolecules 2023, 56, 4835−4844

Table 5. Fitting Results for the Rings R20 at ϕ_R = 10 ww % and R10 at ϕ_R = 15−16 ww % in Different Linear Hosts. $R_{g,R}$ Is a Ring Radius of Gyration; $\chi_{F,RL}$ Is the Flory−Huggins Parameter; ν Is the Fractal Exponent; a4(Q^{-4}) and a2(Q^{-2}) Are Coefficients for the Porod Term (Q^{-4}) and the Q^{-2} Term Describing the Low Q Scattering; and χ^2 Is the Goodness of the Fit[a]

sample	$R_{g,R}$/nm	$-\chi_{F,RL}$	ν	a4(Q^{-4})/nm^4 cm^{-1}	a2(Q^{-2})/nm^2 cm^{-1}	χ^2
R20L2	3.45 ± 0.02	$9.4 \times 10^{-3} \pm 1.4 \times 10^{-4}$	$0.498 \pm 5.5 \times 10^{-4}$	$1.15 \times 10^{-4} \pm 6.7 \times 10^{-6}$		0.79
R20L20	3.46 ± 0.01	$0.0139 \pm 1 \times 10^{-4}$	$0.497 \pm 3.6 \times 10^{-4}$		$0.0258 \pm 2.6 \times 10^{-3}$	2.89
R20L80	3.37 ± 0.02	$0.0128 \pm 8.4 \times 10^{-5}$	$0.491 \pm 4 \times 10^{-4}$		$0.118 \pm 2.57 \times 10^{-3}$	5.51
R20L200[a]	3.46 ± 0.02	$0.0132 \pm 5.9 \times 10^{-5}$	$0.503 \pm 1.3 \times 10^{4}$	$1.68 \times 10^{-6} \pm 7.9 \times 10^{-7}$		39.7
R20 (melt)	2.78 ± 0.1		0.45			
R10L2	2.38 ± 0.02	$0.0139 \pm 1.4 \times 10^{-4}$	$0.493 \pm 7.6 \times 10^{-4}$		$5.31 \times 10^{-3} \pm 2.2 \times 10^{-4}$	1.59
R10L80	2.41 ± 0.01	$0.0094 \pm 1.4 \times 10^{-4}$	$0.493 \pm 7.6 \times 10^{-4}$		$1.2 \times 10^{-2} \pm 1.3 \times 10^{-3}$	1.47
R10 (melt)	2.14 ± 0.04		0.46			

[a]The R20/L200 sample could not be fitted by a combination of Q^{-4} and Q^{-2} terms; instead, the power−law exponent for the low Q contributions was fitted, revealing −3.34 ± 0.11.

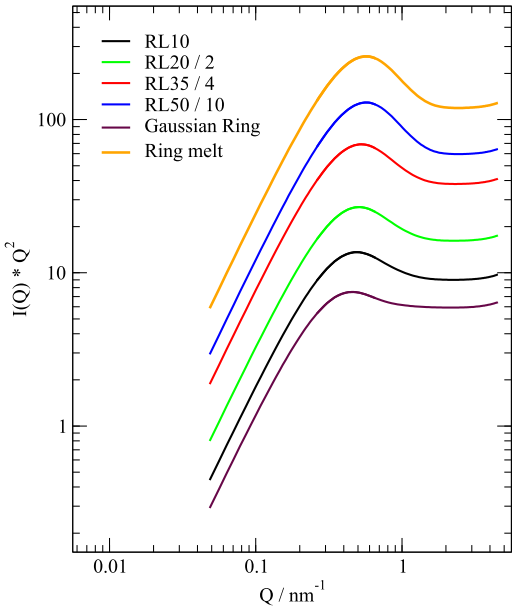

Figure 4. Ring form factors calculated for the samples R40/L100 at different ring volume fractions using the parameters presented in Table 2 (blue: ϕ_R = 50 ww %; red: ϕ_R = 35 ww %; green: ϕ_R = 20 ww %; and black: ϕ_R = 10 ww %); for comparison, the form factors of the Gaussian ring R40 (brown) and the R40 ring in the melt (orange) are also presented. For better visibility, the form factors are shifted by the factors indicated in the insert.

Ring−linear threading events are the key mechanism that governs the size, the conformation, and the dynamics of ring−linear blends. Unfortunately, threading is not directly accessible by scattering techniques, and we have to rely on simulations. According to Tsalikis and Mavrantzas,[35] the number of threadings of rings by linear chains is given by the entanglement number Z of the linear chain and decreases with increasing Z, implying that with increasing Z, the ring swelling is reduced. In contrast, for all linear hosts from L2 to L200 within errors, we found that swelling is not affected by the host length (Table 3). However, the simulation only considered symmetric blends RxLx, and thus, the behavior of asymmetric blends may differ from the symmetric case. Based on their MC simulations that are in agreement with our results, Mo et al. observed that only for short matrices, a significant dependence of ring swelling on the host length occurs.[12] As for the Mavrantzas results, the number of threadings is high.

The dependence of the ring size on the ring volume fraction has been discussed in several simulation works. As alluded to in the Introduction, Iyer et al. suggested a scaling model, where for rings in a linear melt, the ring size stays independent of the ring volume fraction ϕ_R until it reaches the ring−ring overlap concentration $\phi_R^* = \frac{3Nl^3}{4\pi R_{ring}^3}$—here, R_{ring} is the span of the ring—then the ring should shrink according to $R_{ring}(\phi_R) \sim (\phi_R^*)^{2\nu-1}$, where ν is the fractal ring exponent.[13] For the investigated R40 ring, ν = 0.448 and the prediction becomes $R_{ring} \sim \phi_R^{-0.1}$, identical to our result for $\nu = -\frac{0.2}{2} = -0.1$. Considering the overlap concentration for R40 ϕ_R^* = 0.024, all our measurements were taken above ϕ_R^*. Finally, we compare our results for the ring swelling with the simulation results of Halverson et al. In Figure 5, the data for the swelling degree as a function of the ring volume fraction is presented together with the data obtained by Halverson et al. for the rings of different sizes.[36] The simulation results of Halverson et al.[36] come out systematically somewhat larger

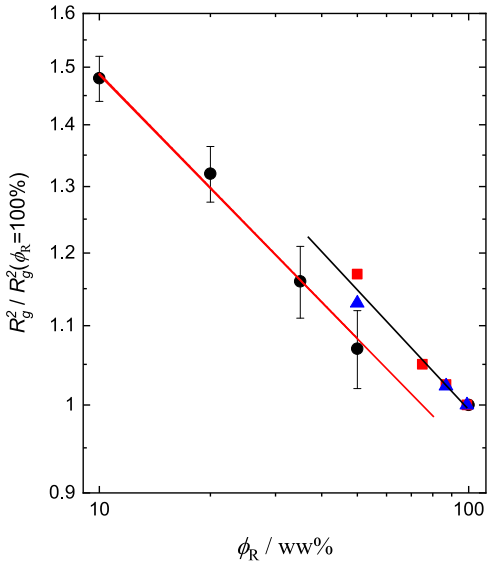

Figure 5. Degree of swelling for the R40 rings as a function of ring concentration blended with the linear chain L100 (black symbols). Blue and red symbols present the literature data for the rings of different sizes (N = 200: red and N = 400: blue) in the linear matrix of equivalent length.[36] The solid lines have a slope of −0.20 (experiment) and −0.21 (simulations).

https://doi.org/10.1021/acs.macromol.2c02444
Macromolecules 2023, 56, 4835−4844

than the experimental data (Figure 5). Also, the slope of $R_{g,R}^2(\phi_R)/R_{g,R}{}^2(\phi_R = 100\ \text{ww}\ \%) \sim \phi_R^{-0.21}$ within statistical errors agrees with the experimental value −0.20.

The only experimental study of large ring−linear blends that we are aware of is the work of Iwamoto et al.[37] on PS rings in linear PS matrices. They studied the ϕ_R dependence of $R_{g,R}^2$ for a 70 kDa PS ring embedded in linear PS matrices of 20, 80, and 270 kDa. Independent of the linear host size, they found $R_{g,R}^2(\phi_R) \sim \phi_R^{-0.1}$, a significantly weaker volume fraction dependence compared to our result of $\nu = -0.2$. Similar to our result that at $\phi_R = 10$ ww % (experimental value $R_{g,R} = 4.61$ nm compared to the Gaussian prediction of 5.19 nm), the PS ring at $\phi_R = 20$ ww % is also found to be still smaller than a Gaussian ring.

Fractal Exponent ν. The fractal exponent ν changes with the concentration of the rings in the linear matrix in a linear fashion (Figure 2d). At lower ring concentrations (10−16 ww %), ν is close to 0.5, indicating a near-Gaussian conformation of the rings. With an increase in the ring volume fraction ϕ_R, ν decreases systematically and reaches the bulk ν value for the R40 ring at the concentration of 50 ww %. This indicates that already at $\phi_R = 50$ ww %, the ring conformation is close to the fractal found in the bulk.

Flory−Huggins Parameter. The RPA applied to the SANS data from the ϕ_R-dependent blends R40/L100 reveal a Flory−Huggins parameter $\chi_{F,RL}$ that is negative (averaged value $\langle\chi_{F,RL}\rangle = -0.0152$) and, within errors, independent of the ring volume fraction. For the R20 ring in hosts of different sizes, the average $\langle\chi_{F,RL}\rangle = -0.0122$ is again negative and independent of the host length. Finally, for R10, we find that $\langle\chi_{F,RL}\rangle = -0.011$. As noted above, with decreasing ring size, the magnitude of $\chi_{F,RL}$ is also diminishing. Thus, $\chi_{F,RL}$ depends on the ring size but is independent of the blend conditions.

A negative Flory−Huggins parameter indicates attraction between the rings and the linear chains, which in turn signalizes ring−ring repulsion. This observation fits well with the simulation results of the Mavrantzas group, who found a strong correlation hole effect between C−C pairs belonging to PEO rings. Thus, linear chains penetrate rings more strongly than rings can penetrate other rings. The center of the mass pair correlation function between rings very nicely demonstrates that rings avoid each other.[8,38] The simulations display an important center of the mass ring−ring correlation hole that becomes more pronounced with increasing ring size.

We note that isotope effects typically lead to χ parameters in the order of magnitude of 10^{-4}, while here, $\chi_{F,RL}$ appears to be nearly 2 orders of magnitude larger. As an example, Bates et al. presented the chi-parameter for a hydrogenated/deuterated (h/d) blend of 1−4 polybutadiene (PB) as $\chi = 0.326T^{-1} - 2.3 \times 10^{-4}$, which for our measurement temperature would give 5.6×10^{-4}, while the topological chi-parameter between rings and linear chains comes out as $\chi \cong -1.5 \times 10^{-2}$.[39] As demonstrated in our recent work,[21] the chi-parameter between h/d rings of similar size is negligible. Thus, the chi-parameter in ring−linear blends is of topological origin and much larger than a possible contribution due to isotope incompatibility.

In order to demonstrate the huge influence of the χ parameter on the experimental results, Figure 6 shows the importance of the χ parameter as well as of the low Q power law contributions. The example shows that $\chi_{F,RL}$ gives rise to an essential correction, which is also true for the other samples.

According to Sakaue,[40] "The miscibility enhancement in ring-linear blend is intuitively understandable in the following way. In a phase-separated state, the concentration of rings in ring-rich phase is high, thus rings there feel strong entropic penalty due to the nonconcatenation TC (topological constraint). The homogenization by mixing provides a way to loosen the TC in rings, *i.e.* the entropic penalty due to nonconcatenation. TC acts as a driving force for mixing."

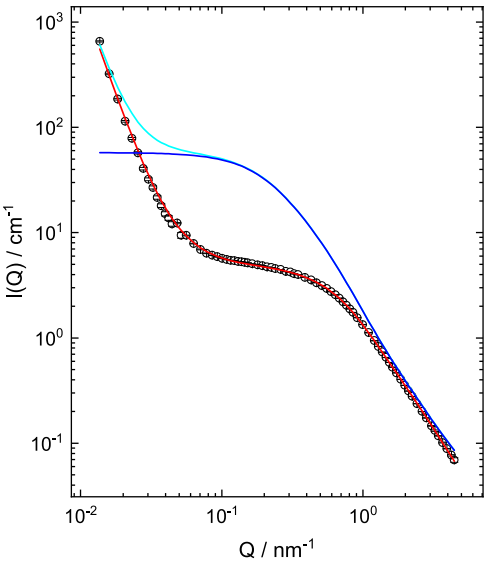

Figure 6. SANS data from R40/L100 at a volume fraction of 50 ww %. The red line displays the result from the RPA fit including the two power laws (Q^{-2} and Q^{-4}). The cyan line presents the calculation of $S(Q)$ setting $\chi_{F,RL} = 0$. Finally, the dark blue line is a result of a RPA calculation with $\chi_{F,RL} = 0$ and without power laws.

Second Q^{-2} Regime. As may be seen from Figure 2b, the data from the R40/L100 blend at different ring volume fractions display an intermediate Q-regime between the ring form factor and the low Q^{-4} Porod scattering; there, a Q^{-2} term emerges, the intensity of which grows linearly with ϕ_R. Here, we investigate this phenomenon in some more detail, in particular also in order to clarify whether a Q^{-3} contribution would also be possible. The best data for this purpose are those from the 50/50 blend. Figure 7 displays the data in the intermediate Q-range $0.04 < Q < 1.0$ nm^{-1}.

From Figure 7, it is obvious that beyond the Porod scattering at low Q (blue line) that probably arises from air bubbles in the high-molecular-weight melt, there is a significant contribution that increases above the Guinier plateau from the rings. This contribution is well described by a Q^{-2} power law indicating correlations between the ring centers of mass that follow Gaussian random walk statistics.

In order to investigate whether a mass−fractal-type correlation that would follow a Q^{-3} power law could also explain the intermediate Q-regime, we performed the same investigation, now imposing a Q^{-3} intermediate scattering behavior. Figure 8 displays the result.

It is obvious that in the Q-range below $Q = 0.1$ nm^{-1}, the fit misses the proper increase in the structure factor. Thus, apparently the correlation between the ring centers—at the investigated low Q, the rings appear point-like—is best described by Gaussian random walk statistics leading to Q^{-2} contribution.

Could such a correlation be mediated by the long linear chains that thread the rings? However, since each ring is threaded by several linear chains—from simulations, one

https://doi.org/10.1021/acs.macromol.2c02444
Macromolecules 2023, 56, 4835−4844

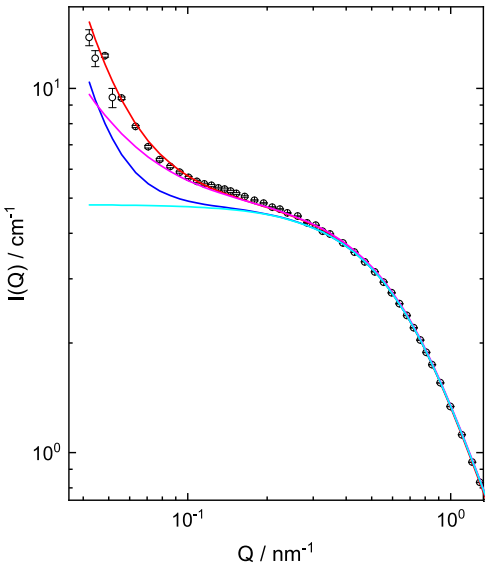

Figure 7. SANS data from the R40/L100 50 ww % sample in the intermediate Q-regime; red line: full fit including a Q^{-2} and a Q^{-4} contribution; magenta line: Q^{-2} contribution only; blue line: Q^{-4} contribution; and cyan line: RPA result from the ring−linear melt.

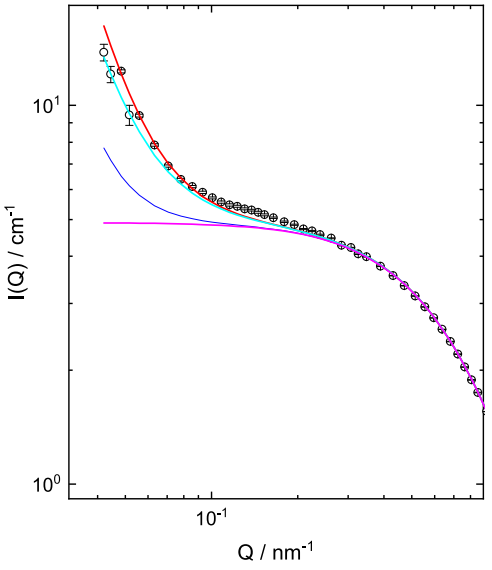

Figure 8. SANS data from the R40/L100 50 ww % blend in the intermediate Q-regime; red line: full fit including a Q^{-3} and a Q^{-4} contribution; cyan line: Q^{-3} contribution only; blue line: Q^{-4} contribution; and magenta line: RPA result from the ring−linear melt.

would estimate about 10 linear chains—we would have expected that the rings would act like crosslinks in a temporary network. Such crosslinks would lead to a mass fractal arrangement, which we do not see. Furthermore, how can temporary correlations, *e.g.*, due to threading, impose such correlation in a SANS snapshot?

Finally, could the Q^{-2} term indicate a looming phase transition, where rings and linear chains would separate? With a negative $\chi_{F,RL}$ on the local monomer scale, this could be excluded. However, there might be a nonlocal component $\chi_{F,RL}$ that becomes positive at large distances. In the following, we present an estimate on the possibly underlying critical fluctuations or domain sizes based on recent diffusion experiments on ring−linear blends.[41] In diffusion experiments on ring−linear blends in particular, we studied a blend of a 20 K ring in an 80 K matrix. The diffusion studies resulted in the observation of two diffusion modes, a slow expected one and a fast mode, which is still not understood. One possible explanation for the fast mode was the existence of a ring-rich phase, where the dominant treading is onefold. The ring-rich phase could be related to either a domain or a large wavelength critical fluctuation. At the temperature T = 413 K of the SANS measurements, the diffusion coefficients were $D_{slow} = 6.86 \times 10^{-16}$ and $D_{fast} = 5.05 \times 10^{-14}$ m^2/s. These values have to be rescaled for our conditions of a 40 K ring in a 100 K matrix. For the fast mode, the theoretical prediction for a once-threaded ring that quantitatively was very close to our results amounts to

$$D_{fast} = \frac{8}{15} D_0 \frac{N_e}{N_R N_L} \tag{7}$$

where D_0 is the monomeric diffusivity and N_e is the entanglement molecular weight. Transcribing D_{fast} to the values of our structural studies yields a correction factor of 2.5. Thus, $D_{fast} = 2.0\ 10^{-14}$ m^2/s.

The evaluation with the two-state model of Kärger[42,43] that considers exchanges between areas characterized by fast and slow diffusion, respectively, yielded a life time of the fast diffusive state of $\tau_{fast} \gg 1$ s. For an estimate, let us take τ_{fast} = 10 s. With this assumption, we may calculate the mean-squared displacement of a ring in the fast mode

$$\langle r^2 \rangle \cong 6 D_{fast} \tau_{fast} \tag{8}$$

yielding $\langle r^2 \rangle \cong 10^6$ nm^2 or $\sqrt{\langle r^2 \rangle} \cong 1\ \mu$m. Thus, the typical wavelength of a critical fluctuation would be of about this size or larger; similarly, microphase-separated regions would also be at least in this order.

We may conclude that the observation of a Q^{-2} increase in the SANS intensities at very low Q is at least compatible with such a scenario. On the other hand, why is the χ_F on the scale of the rings negative and how does it become positive for very small Q? Diffusion measurement on the time scale of 1−2 s, possibly using a fluorescent labeling, might shed light on this problem.

SUMMARY AND CONCLUSIONS

In this work, we have presented a systematic investigation of ring−linear blends, where we varied either the ring volume fraction for a given ring in a long linear matrix or the matrix length for a low ring fraction. The following results stand out:

(i) The ring radius of gyration shrinks with increasing ring fraction and nearly reaches the $R_{g,R}$ of the ring melt at a volume fraction of ϕ_R = 50 ww %. At the same time, the fractal dimension, which is close to a Gaussian conformation at low ϕ_R, decreases to the value of the ring melt.

(ii) Aside from very short matrices, the ring size is independent of the host length.

(iii) Following an RPA treatment, the Flory−Huggins parameter comes out negative and independent of ϕ_R, signifying ring−linear attraction that leads to ring−ring repulsion.

(iv) $\chi_{F,RL}$ decreases with decreasing ring size, which might be related to the decreasing possibility of threading events, when the ring size becomes smaller.

https://doi.org/10.1021/acs.macromol.2c02444
Macromolecules 2023, 56, 4835−4844

(v) The volume fraction-dependent data at low Q in between the Guinier plateau of the ring form factor and the very low Q Porod scattering displays a Q^{-2} intensity regime, the intensity of which increases proportional to ϕ_R.

(vi) The origin of this Q^{-2} contribution is not clear but may be related to critical fluctuations or microphase separation induced by a nonlocal positive contribution to $\chi_{F,RL}$.

(vii) Another interpretation may be that threading by linear chains causes ring−ring correlations following random walk statistics.

The experimental results fit well into the general picture that is mainly based on simulations, even though in detail, quantitative differences are obvious. Finally, our results are in qualitative agreement with earlier studies on PS ring−linear blends.

AUTHOR INFORMATION

Corresponding Author

Margarita Kruteva − *Jülich Center for Neutron Science (JCNS), Forschungszentrum Jülich GmbH, Jülich 52425, Germany;* orcid.org/0000-0002-7686-0934; Email: m.kruteva@fz-juelich.de

Authors

Michael Monkenbusch − *Jülich Center for Neutron Science (JCNS), Forschungszentrum Jülich GmbH, Jülich 52425, Germany;* orcid.org/0000-0001-6733-832X

Jürgen Allgaier − *Jülich Center for Neutron Science (JCNS), Forschungszentrum Jülich GmbH, Jülich 52425, Germany;* orcid.org/0000-0002-9276-597X

Wim Pyckhout-Hintzen − *Jülich Center for Neutron Science (JCNS), Forschungszentrum Jülich GmbH, Jülich 52425, Germany;* orcid.org/0000-0002-1142-359X

Lionel Porcar − *Institut Max von Laue-Paul Langevin (ILL), Grenoble F-38042, France*

Dieter Richter − *Jülich Center for Neutron Science (JCNS), Forschungszentrum Jülich GmbH, Jülich 52425, Germany*

Complete contact information is available at: https://pubs.acs.org/10.1021/acs.macromol.2c02444

Notes

The authors declare no competing financial interest.

ACKNOWLEDGMENTS

We acknowledge Barbara Gold and Sebastian Gooßen for SANS experiments on R10 and R20 samples.

REFERENCES

(1) Cremer, T.; Cremer, C. Chromosome Territories, Nuclear Architecture and Gene Regulation in Mammalian Cells. *Nat. Rev. Genet.* **2001**, *2*, 292−301.

(2) Mirny, L. A. The Fractal Globule as a Model of Chromatin Architecture in the Cell. *Chromosome Res.* **2011**, *19*, 37−51.

(3) Ge, T.; Panyukov, S.; Rubinstein, M. Self-Similar Conformations and Dynamics in Entangled Melts and Solutions of Nonconcatenated Ring Polymers. *Macromolecules* **2016**, *49*, 708−722.

(4) Grosberg, A. Y. Annealed Lattice Animal Model and Flory Theory for the Melt of Non-Concatenated Rings: Towards the Physics of Crumpling. *Soft Matter* **2014**, *10*, 560−565.

(5) Obukhov, S.; Johner, A.; Baschnagel, J.; Meyer, H.; Wittmer, J. P. Melt of Polymer Rings: The Decorated Loop Model. *Europhys. Lett.* **2014**, *105*, 48005.

(6) Rubinstein, M. Dynamics of Ring Polymers in the Presence of Fixed Obstacles. *Phys. Rev. Lett.* **1986**, *57*, 3023−3026.

(7) Kruteva, M.; Allgaier, J.; Monkenbusch, M.; Porcar, L.; Richter, D. Self-Similar Polymer Ring Conformations Based on Elementary Loops: A Direct Observation by SANS. *ACS Macro Lett.* **2020**, *9*, 507−511.

(8) Tsalikis, D. G.; Mavrantzas, V. G. Size and Diffusivity of Polymer Rings in Linear Polymer Matrices: The Key Role of Threading Events. *Macromolecules* **2020**, *53*, 803−820.

(9) Papadopoulos, G. D.; Tsalikis, D. G.; Mavrantzas, V. G. Microscopic Dynamics and Topology of Polymer Rings Immersed in a Host Matrix of Longer Linear Polymers: Results from a Detailed Molecular Dynamics Simulation Study and Comparison with Experimental Data. *Polymers* **2016**, *8*, 283.

(10) O'Connor, T. C.; Ge, T.; Grest, G. S. Composite Entanglement Topology and Extensional Rheology of Symmetric Ring-Linear Polymer Blends. *J. Rheol.* **2022**, *66*, 49−65.

(11) Hagita, K.; Murashima, T. Molecular Dynamics Simulations of Ring Shapes on a Ring Fraction in Ring-Linear Polymer Blends. *Macromolecules* **2021**, *54*, 8043−8051.

(12) Mo, J.; Wang, J.; Wang, Z.; Lu, Y.; An, L. Size and Dynamics of a Tracer Ring Polymer Embedded in a Linear Polymer Chain Melt Matrix. *Macromolecules* **2022**, *55*, 1505−1514.

(13) Iyer, B. V. S.; Lele, A. K.; Shanbhag, S. What Is the Size of a Ring Polymer in a Ring-Linear Blend? *Macromolecules* **2007**, *40*, 5995−6000.

(14) Jeong, C.; Douglas, J. F. Relation between Polymer Conformational Structure and Dynamics in Linear and Ring Polyethylene Blends. *Macromol. Theory Simul.* **2017**, *26*, 1700045.

(15) Iwamoto, T.; Doi, Y.; Kinoshita, K.; Takano, A.; Takahashi, Y.; Kim, E.; Kim, T. H.; Takata, S. I.; Nagao, M.; Matsushita, Y. Conformations of Ring Polystyrenes in Semidilute Solutions and in Linear Polymer Matrices Studied by SANS. *Macromolecules* **2018**, *51*, 6836−6847.

(16) Vlahos, C.; Kosmas, M. Effective Interaction Parameters of Star/Star, Ring/Ring, and Ring/Linear Chemically Identical Blends. *Macromolecules* **2004**, *37*, 9184−9190.

(17) Kobayashi, Y.; Doi, Y.; Abdul Rahman, S. S.; Kim, E.; Kim, T.-H.; Takano, A.; Matsushita, Y. SANS Study of Ring Topology Effects on the Miscibility of Polymer Blends. *Macromolecules* **2018**, *51*, 1885−1893.

(18) Bensafi, A.; Maschke, U.; Benmouna, M. Cyclic Polymers in Good Solvents. *Polym. Int.* **2000**, *49*, 175−183.

(19) Hammouda, B. Probing Nanoscale Structures−the Sans Toolbox. *NIST Cent. Neutron Res.* **2010**, *224*, 307−309.

(20) Hövelmann, C. H.; Gooßen, S.; Allgaier, J. Scale-Up Procedure for the Efficient Synthesis of Highly Pure Cyclic Poly(Ethylene Glycol). *Macromolecules* **2017**, *50*, 4169−4179.

(21) Kruteva, M.; Allgaier, J.; Monkenbusch, M.; Hoffmann, I.; Richter, D. Structure and Dynamics of Large Ring Polymers. *J. Rheol.* **2021**, *65*, 713−727.

(22) Gooßen, S.; Krutyeva, M.; Sharp, M.; Feoktystov, A.; Allgaier, J.; Pyckhout-Hintzen, W.; Wischnewski, A.; Richter, D. Sensing Polymer Chain Dynamics through Ring Topology: A Neutron Spin Echo Study. *Phys. Rev. Lett.* **2015**, *115*, 148302.

(23) Gold, B. J.; Pyckhout-Hintzen, W.; Wischnewski, A.; Radulescu, A.; Monkenbusch, M.; Allgaier, J.; Hoffmann, I.; Parisi, D.; Vlassopoulos, D.; Richter, D. Direct Assessment of Tube Dilation in Entangled Polymers. *Phys. Rev. Lett.* **2019**, *122*, 088001.

(24) https://www.ill.eu/users/instruments/instruments-list/d22/description/instrument-layout.

(25) Kruteva, M.; Allgaier, J.; Grillo, I.; Hoffmann, I.; Porcar, L.; Richter, D.; Schweins, R. Self Similar Dynamics of Ring Polymers. Institut Laue-Langevin, 1895.

(26) Strunz, P.; Mortensen, K.; Janssen, S. SANS-II at SINQ: Installation of the Former Risø-SANS Facility. *Phys. B Condens. Matter* **2004**, *350*, E783−E786.
(27) Feoktystov, A. V.; Frielinghaus, H.; Di, Z.; Jaksch, S.; Pipich, V.; Appavou, M. S.; Babcock, E.; Hanslik, R.; Engels, R.; Kemmerling, G.; Kleines, H.; Ioffe, A.; Richter, D.; Brückel, T. KWS-1 High-Resolution Small-Angle Neutron Scattering Instrument at JCNS: Current State. *J. Appl. Crystallogr.* **2015**, *48*, 61−70 urn:issn:1600-5767.
(28) De Gennes, P. G. *Scaling Concepts in Polymer Physics*; Cornell University Press: Ithaca and London, 1979.
(29) Kirste, R. G.; Lehnen, B. R. Die Bestimmung Des Chemischen Potentials Und Des Expansionskoeffizienten in Mischungen von Polydimethylsiloxanen Unterschiedlichen Molekulargewichts. *Die Makromol. Chem.* **1976**, *177*, 1137−1143.
(30) Tangari, C.; Ullman, R.; King, J. S.; Wignall, G. D. Small-Angle Neutron Scattering from Bimodal Melts of Polystyrene. *Macromolecules* **1990**, *23*, 5266−5269.
(31) Landry, M. R. Scaling Behavior of Swollen Chains in Bimodal Molecular Weight Blends. *Macromolecules* **1997**, *30*, 7500−7510.
(32) Lang, M.; Rubinstein, M.; Sommer, J. U. Conformations of a Long Polymer in a Melt of Shorter Chains: Generalizations of the Flory Theorem. *ACS Macro Lett.* **2015**, *4*, 177−181.
(33) Torikai, N.; Takabayashi, N.; Suzuki, J.; Noda, I.; Matsushita, Y. SANS Study on Chain Dimension of Polystyrenes Diluted with Low Molecular-Weight Homologues in Semi-Dilute Solutions. *Polymer* **2013**, *54*, 929−934.
(34) Torikai, N.; Takabayashi, N.; Noda, I.; Suzuki, J.; Matsushita, Y. Chain Dimensions of Polystyrenes Diluted with Low Molecular Weight Homologues. *J. Phys. Chem. Solids* **1999**, *60*, 1325−1328.
(35) Tsalikis, D. G.; Mavrantzas, V. G. Threading of Ring Poly(Ethylene Oxide) Molecules by Linear Chains in the Melt. *ACS Macro Lett.* **2014**, *3*, 763−766.
(36) Halverson, J. D.; Grest, G. S.; Grosberg, A. Y.; Kremer, K. Rheology of Ring Polymer Melts: From Linear Contaminants to Ring-Linear Blends. *Phys. Rev. Lett.* **2012**, *108*, 038301.
(37) Iwamoto, T.; Doi, Y.; Kinoshita, K.; Ohta, Y.; Takano, A.; Takahashi, Y.; Nagao, M.; Matsushita, Y. Conformations of Ring Polystyrenes in Bulk Studied by SANS. *Macromolecules* **2018**, *51*, 1539−1548.
(38) Khokhlov, A. R.; Nechaev, S. K. Topologically Driven Compatibility Enhancement in the Mixtures of Rings and Linear Chains. *J. Phys. II* **1996**, *6*, 1547−1555.
(39) Bates, F. S.; Wignall, G. D.; Koehler, W. C. Critical Behavior of Binary Liquid Mixtures of Deuterated and Protonated Polymers. *Phys. Rev. Lett.* **1985**, *55*, 2425−2428.
(40) Sakaue, T. Statistical Physics of Ring Polymers Based on Topological Volume Concept. *React. Funct. Polym.* **2019**, *134*, 150−155.
(41) Kruteva, M.; Allgaier, J.; Richter, D. Direct Observation of Two Distinct Diffusive Modes for Polymer Rings in Linear Polymer Matrices by Pulsed Field Gradient (PFG) NMR. *Macromolecules* **2017**, *50*, 9482−9493.
(42) Kärger, J. Zur Bestimmung Der Diffusion in Einem Zweibereichsystem Mit Hilfe von Gepulsten Feldgradienten. *Ann. Phys.* **1969**, *479*, 1−4.
(43) Kärger, J. Der Einfluß Der Zweibereichdiffusion Auf Die Spinechodämpfung Unter Berücksichtigung Der Relaxation Bei Messungen Mit Der Methode Der Gepulsten Feldgradienten. *Ann. Phys.* **1971**, *482*, 107−109.

https://doi.org/10.1021/acs.macromol.2c02444
Macromolecules 2023, 56, 4835−4844